*Annals of GIS*
Vol. 17, No. 1, March 2011, 31–42

Taylor & Francis
Taylor & Francis Group

# The impact of image and class structure upon sub-pixel mapping accuracy using the pixel-swapping algorithm

Peter Luciani* and Dongmei Chen

*Department of Geography, Queen's University, Kingston, Ontario, Canada*

(*Received 18 November 2010; final version received 19 December 2010*)

A series of tests assess the impact of image and class structure within input imagery upon the accuracy of outputs from the pixel-swapping algorithm (PSA) to better assess the viability of this sub-pixel mapping algorithm to spatially locate class proportions and improve soft classification accuracies. Simulated maps with known spatial autocorrelation, class proportion and mixed pixel percentages are sub-pixel mapped at varying zoom factors using the PSA and accuracies measured. Block majority filtering (BMF) of input images is an experimental accuracy control. Results quantify PSA accuracies compared to the BMF based on the interrelationship between spatial autocorrelation, class proportions, zoom factor and mixed pixel quantities. Findings, while validating the known positive correlation between spatial autocorrelation and PSA accuracy, demonstrate class proportion difference and mixed pixel quantities to be positively and negatively related to PSA accuracy, respectively. Class proportion affects PSA accuracy to a greater degree on maps exhibiting low spatial autocorrelation levels versus maps with high spatial autocorrelation levels. Traditional accuracy measures, such as overall accuracy, are shown to overestimate the true performance of the PSA. The difference in overall accuracy of the PSA between all map pixels and within mixed map pixels alone can be over 20%. Overall, in general, the PSA accurately sub-pixel mapped input images with an approximate minimum level of spatial autocorrelation at a *Moran's I* of 0.63, a maximum of 30% of mixed pixels relative to entire image pixels, a difference in class proportions greater than 40% and at zoom factors below 10.

**Keywords:** sub-pixel mapping; pixel-swapping algorithm; image structure; accuracy; spatial auto correlation; mixed pixels



## 1. Introduction and background

The mixed pixel problem is prevalent within moderate spatial resolution satellite imagery when process and observation scales (Blöshchl and Sivapalan 1995) are mismatched. The problem arises when the spectral response of a given pixel comprises multiple endmembers. These endmembers represent multiple land cover classes that vary on the ground at a spatial frequency not captured at the sensor's spatial resolution. Mixed pixels are a major problem to image classification causing errors in estimating land cover area and distribution within 'hard' classified maps across scales (Lu and Weng 2007).

Compared with traditional hard classification, soft classification methods have the advantage of estimating the proportions of land cover classes to spectral end members, and thus, capturing multiple land covers within mixed pixels. However, soft classification fails to account for the spatial location and distribution of land cover proportions within pixels (Kasetkasem *et al.* 2005). To this end several approaches, termed sub-pixel mapping, super-resolution mapping (Atkinson 2005) or downscaling (Boucher and Kyriakidis 2006), have been developed to spatially distribute and map at finer spatial resolutions class proportions that have been derived by 'soft' classification. The ability of these algorithms to do so can enhance spatial resolution and accuracy of remote sensing classification, notably, upon moderate spatial resolution imagery, that while still being susceptible to mixed pixels, affords beneficial and cost-effective spatial and temporal coverage not offered by higher spatial resolution imagery.

Of a suite of sub-pixel mapping algorithms (e.g. Gavin and Jennison 1997, Foody 1998, Tatem *et al.* 2001, Verhoeye and De Wulf 2002, Atkinson 2005, Mertens *et al.* 2004, 2006, Boucher and Kyriakidis 2006), the pixel-swapping algorithm (PSA) (Atkinson 2005) is the first to be applied for sub-pixel mapping based solely on the output from soft classification (Atkinson *et al.* 1997). The PSA is considered simple, computationally efficient and accurate and exhibits potential to improve satellite imagery classification efforts as is evident in Makido and Qi (2005), Makido and Shortridge (2005), Muslim *et al.* (2006) and Thornton *et al.* (2006). However, these authors only provide preliminary evidence of the influence of PSA settings under a limited set of image and class structure factors

*Corresponding author. Email: 5pdl@queensu.ca

ISSN 1947-5683 print/ISSN 1947-5691 online

DOI: 10.1080/19475683.2011.558022
http://www.informaworld.com

(i.e. spatial autocorrelation and class frequency distribution) upon PSA performance. With the PSA functioning by maximizing spatial autocorrelation, this input image metric has a known positive relation to the accuracy of PSA output maps as per Makido and Qi (2005) and Makido and Shortridge (2005). To date there has been no analysis of the interrelationship, across a broader range, of these and additional factors that directly impact PSA performance and accuracy. Furthermore, PSA performance has not been assessed specifically within mixed pixels, where the PSA is truly functioning and put to the test.

Other research, employing the PSA, highlights additional research gaps. Previous PSA applications have focused on achieving higher overall accuracies through sub-pixel mapping of binary multiple land cover classes (Atkinson 2005, Muslim *et al.* 2006, Thornton *et al.* 2006). Classes are derived from soft-classified remote sensing imagery and applied in the PSA. The research acknowledges the need for a minimum level of spatial autocorrelation in the classified imagery for the PSA to function and produce useful results. However, to date, this minimum level is not established in conjunction with image and class structure factors within input imagery and resulting PSA output accuracy. Such knowledge aids in determining when the PSA is worthwhile to use to improve overall classification results based on expected accuracy gains. Also, overall accuracy (OA) or percent correctly classified (PCC) values of all pixels are convention to assess the accuracy of the PSA outputs. This accuracy measure potentially overestimates the performance of PSA by including both pure pixels and mixed pixels. If a pixel is pure, all sub-pixels are assigned to one class and sub-pixel mapping is purely geometric with no pixel-swapping taking place. Sub-pixel mapping is thus warranted only within mixed pixels, and in this study pure and mixed pixels are consequently identified and accuracies of the PSA's ability to sub-pixel map within these pixel types evaluated.

PSA applications (Atkinson 2005, Muslim *et al.* 2006, Thornton *et al.* 2006) have also relied on a finer resolution classified image existing with a predefined set of class labels deemed as 'accurate'. Such a reference map is used to assess the positional and classification accuracies of images generated by the PSA. In reality such imagery is not always available. Accordingly, in the absence or limited availability of reference imagery, isolating accuracy limits of the PSA as a function of image and class structures is beneficial. Again, with this information practitioners are better able to ascertain if sub-pixel mapping is meritorious based on the expected improvement in accuracy potentially gained by sub-pixel mapping given the spatial and class structure within input imagery or regions/zones thereof.

The purpose of this research is to systematically assess the accuracy of the PSA, across varying algorithm settings, to regenerate synthetic reference imagery that replicates a typical and broad range of class variability and image structure within mixed and overall pixels of an entire or portions of classified remotely sensed maps. All the images employed and generated in this research are termed 'maps' holding thematic classes per classified remotely sensed imagery. The class and image structure metrics include class spatial and frequency distributions/proportion, spatial autocorrelation/dependence levels, mixed versus pure pixel distributions and zoom factors (defined in Section 2).

The impact of these factors and PSA settings upon the accuracy of PSA output maps is examined. The inputs to the algorithm are generated by degrading binary reference maps existing at finer spatial resolutions to class proportion maps at coarser spatial resolutions. In this manner, the influence of soft classification error on final accuracy is eliminated and the true accuracy of the PSA is isolated. As a result, findings help illuminate cumulative error in the image-processing chain. The outputs from PSA are compared with those generated from a simple block majority filtering or mapping approach. OA, individual producer (PA) and user (UA) class accuracies define the accuracy of the generated maps.

## 2. The pixel-swapping algorithm

The PSA is based on the assumption of maximum class autocorrelation at the target resolution, or to simply maximize spatial dependence (Matheron 1965, Goovaerts 1997, Curran and Atkinson 1998, Chiles and Delfiner 1999) or autocorrelation amongst neighbouring binary classified sub-pixels derived from the pixels of coarse image fractions/proportions from soft classified imagery. To establish the number of sub-pixels, which defines the extent of sub-pixel mapping or the target resolution of the output map, a zoom factor is set. Zoom factor is the setting in the PSA defining a base number to power 2 to express the number of sub-pixels to be generated. For example, a zoom factor of 2 results in 4 sub-pixels or alternatively a zoom factor of 10 results in 100 sub-pixels. In relation to the spatial resolution of typical classified remotely sensed image such as Landsat imagery at 30 m spatial resolution, the mentioned zoom factors result in spatial resolutions of output imagery at 15 m and 3 m, respectively.

The PSA maps the optimum spatial arrangement of the sub-pixels by iteratively and deterministically swapping these binary classified sub-pixels. This mapping continues until maximum spatial autocorrelation is achieved based on their 'attractiveness' as a distance weighted function of their neighbours. To perform this task, the PSA initially ranks the attractiveness of each sub-pixel location either 1 (least attractive) or 0 (most attractive) as a distance-weighted function of its neighbours based on an arbitrary sub-pixel arrangement. For every sub-pixel its attractiveness *Oi* is calculated as a distance weighted function of its neighbours:

| | | | | |
|---|---|---|---|---|
| 1 | 2 | 3 | 4 | 5 |
| 16 | 17 | 18 | 19 | 6 |
| 15 | 24 | $\mathbf{X}_i$ | 20 | 7 |
| 14 | 23 | 22 | 21 | 8 |
| 13 | 12 | 11 | 10 | 9 |

Figure 1. Pixel-swapping algorithm number of neighbour ($n$) setting configuration.

$$O_i = \sum_{j=1}^{n} \lambda_{ij} z(\mathrm{x}_j) \tag{1}$$

where $n$ is the number of neighbours based on a selected neighbouring distance depth of sub-pixels. The neighbourhood configuration is a square block comprising sub-pixels (as numbered) at a specified distance depth from all four sides of the subject sub-pixel ($Xi$) at the centre or foci of the neighbourhood (e.g., neighbour depth of 2 equates to an ($n$) of 24 neighbours as conceptualized in Figure 1). Higher depth settings simply increase the number of neighbours in successive rings of sub-pixels in the square block configuration. $Z(\mathrm{x}_j)$ is the value of the (binary) class $z$ at the $j$th pixel location $\mathrm{x}_j$, and $\lambda_{ij}$ is a weight derived as:

$$\lambda_{ij} = \exp\left(\frac{-h_{ij}}{a}\right) \tag{2}$$

where $h_{ij}$ is the distance between the pixel location for which the attractiveness is desired $\mathrm{x}_i$ and the location of the neighbour $\mathrm{x}_j$, and $a$ is the effective distance of pixels in geostatistical terms expressed as a non-linear pixel distance parameter in the exponential weighting function or model of the PSA (Atkinson 2005).

The exponential weighting function chosen here is essentially arbitrary but follows Atkinson (2005). Makido and Shortridge (2005) have applied simple inverse distance weighting function or a Gaussian model.

Once the attractiveness of each sub-pixel location has been predicted based on the current arrangement of sub-pixel classes the optimization algorithm ranks the scores on a *pixel-by-pixel* basis. For each pixel, the least attractive location currently allocated to a '1' (i.e. a '1' surrounded mainly by '0's) is stored. Similarly, the most attractive location currently allocated to a '0' (i.e. a '0' surrounded mainly by '1's) is also stored. If the attractiveness of the least attractive location is less than that of the most attractive location then the classes are swapped for the pixel in question. If it is more attractive, no change is made. Pixels are iteratively swapped to equalize attractiveness across locations based on the spatial autocorrelation within and between pixels. The swapping terminates once the theoretical optimum arrangement is reached or a predefined number of iterations is completed.

Several parameters impact the performance of PSA, including the number of iterations that are successive runs of algorithm whereby pixels are swapped to maximize spatial autocorrelation; and the range ($a$) in the exponential weighting function of the PSA and alternative weighting function models (Atkinson 2005).

Makido and Qi (2005) optimize the number of iterations, range and test the original Atkinson and alternative weighting function models (i.e. Gaussian, inverse distance weighting, and equal weight) within the PSA under varying zoom factors. Overall accuracies expressed as percent correctly classified (PCC) circumvent soft classification error by employing a binary land cover map (forest and non-forest) resampled from a simple sum aggregation, as the reference image. The authors conclude, based on the underlying premise of the PSA to maximize spatial autocorrelation and given that all landscapes are not contiguous, that the degree of spatial autocorrelation of landscapes should be incorporated into the PSA. The minimum level of spatial autocorrelation required by the PSA remains undetermined.

Makido and Shortridge (2005) optimize range and iterations versus zoom factors measured by the same PCC metric under the same alternative weighting function models as Makido and Qi (2005). Two reference images with the same level of spatial autocorrelation, measured by *Moran's I* (Moran 1948), and class frequency distributions are applied, yet under different spatial distributions. The authors demonstrate that when these input images are resampled at decreasing image resolutions, the subsequent *Moran's I* values of the images dropped and this affected sub-pixel mapping efficacy notably as zoom factors increased. The number of iterations, the range ($a$) and the neighbour depth ($n$) settings in the PSA applied here are guided by the work of Atkinson (2005), Makido and Qi (2005) and Makido and Shortridge (2005).

## 3. Data and method

The PSA's performance is assessed on simulated binary maps considering a number of image structure factors at varying PSA parameter settings. Simulated images are used instead of real images as a series of classified and reference images with controlled levels of spatial autocorrelation and class proportion are difficult to obtain as reference maps. In real images, it is hard to control the spatial autocorrelation and error percentage, which makes systematic analysis difficult. Through simulated images, the level of spatial autocorrelation is controlled and constant errors across all images produced. In this manner, any differences in the output are due to only the changes in the controlled factors. Simulated maps also eliminate

the impact of other factors such as classification error and inherent image uncertainty in sensor-derived reference maps. Therefore, to identify and isolate the accuracy of the PSA simulated maps are utilized.

The image structure factors in this analysis include (1) spatial autocorrelation of classes; (2) class proportion; and (3) percentage of sub-pixels in reference maps falling within mixed and pure pixels of spatially aggregated reference maps as input to the PSA (herein referred to as mixed and pure pixel percentages). PSA parameter settings are range ($a$), neighbour depth and zoom factors. Overall, the accuracy limits of the PSA are deduced through running the PSA at varying settings upon input maps derived by coarsening binary reference maps exhibiting a range of image and class structures. Resulting overall, producer and user accuracies of the PSA outputs are documented.

The study is conducted in the following stages as discussed in succeeding sub-sections:

(1) preparing reference maps with different spatial autocorrelation and class proportions;
(2) running PSA sub-pixel mapping tests;
(3) conducting an accuracy assessment.

### 3.1. Preparing reference maps with different spatial autocorrelation and class proportions

In this step a series of reference maps are simulated and spatially aggregated with different spatial autocorrelation levels and class proportions. The PSA only functions upon binary maps that contain two classes (‘1’ and ‘0’). Accordingly, six 500 × 500 pixel binary maps with different class proportions and spatial autocorrelation levels are generated. The systematic process of generating these maps is detailed in Chen and Wei (2009). These maps are illustrated in Figure 2 and the configuration details in Table 1. The maps comprise a set of low, medium and high spatial autocorrelation and class proportion levels. Spatial autocorrelation is measured using *Moran's I*. *Moran's I* values range from below 0.20 on low spatial autocorrelation maps to over 0.80 on highly autocorrelated maps. Mid-range spatial autocorrelation maps exhibit values around 0.58. High class proportion difference maps possess 90% of pixels as class ‘1’ and 10% as class ‘0’. Maps with moderate class differences exhibit 70% of pixels assigned to class ‘1’ and 30% to class ‘0’. The low class difference maps have a close proportion between the two classes – approximately 60% of pixels as class ‘1’ and 40% of pixels as class ‘0’. The naming convention, for example $MH_{37}$, denotes a map of medium high spatial autocorrelation with class proportions of approximately 30% (0's) and 70% (1's) as detailed for all maps in the description column of Table 1.

To run the PSA, the binary reference maps with different spatial heterogeneity and structures are spatially aggregated at coarsening factors of 2, 4 and 10, which correspond to the zoom factors being applied in later runs of the PSA. These zoom factors are selected to represent an expected and reasonable range of resolution enhancement in sub-pixel mapping endeavours based on the success of the majority of PSA applications and tests to date, which have employed zoom factors of 3 (Makido and Qi 2005), 5 (Makido and Qi 2005, Makido and Shortridge 2005, Thornton *et al.* 2006), 7 (Atkinson 2005, Makido and Shortridge 2005) and 10 (Thornton *et al.* 2007). Zoom factors less than 2 may offer little enhancement whereas those greater than 10, which result in greater than 100 sub-pixels from one input image pixel, may produce inaccurate results. Therefore, the zoom factor of 10 has been selected to provide an initial gauge of the PSA's performance at a zoom factor considered an upper limit in practical application of the PSA. The value assigned to the aggregated output map cells here is simply the sum of sub-pixels of class ‘1’ within each pixel in the aggregated maps. This sum replicates a class proportion or fraction from a pseudo-soft classification at the given resolution as necessary input to the PSA.

### 3.2. PSA sub-pixel mapping tests

A number of PSA runs or tests gauge the effect of map and class structure and PSA settings upon the accuracy of maps generated by the PSA. Four test groups executed at zoom factors of 2, 4 and 10 deduce the PSA's performance based on the impact of (1) PSA settings; (2) spatial autocorrelation; (3) class proportions; and (4) mixed versus overall pixel distribution within input maps.

The PSA setting optimums are validated by running the PSA upon high and low spatial autocorrelation maps ($H_{46}$ and $L_{46}$) under a number of settings for each of the zoom factors 2, 4 and 10 and accuracy trend documented. The neighbour depth settings tested are 2 ($n = 24$), 4 ($n = 90$), 6 ($n = 178$) and 8 ($n = 298$) pixels. The ‘range’ ($a$) settings tested are 2, 5, 7 and 9. The optimum settings for each zoom factor are the setting combinations that result in the highest OA. These neighbour depth and range settings and the number of iterations (set at 18) applied in running the PSA are according to optimums and prior research by Atkinson (2005), Makido and Qi (2005) and Makido and Shortridge (2005).

The remaining tests are run at the optimums established and reveal the impact of spatial autocorrelation, class frequency/proportion and sub-pixel distribution amongst mixed and pure pixels. The tests, in this manner, reveal accuracy trend and thresholds under a typical range of input imagery structure variation and PSA settings.

### 3.3. Accuracy assessment

To assess the accuracy of the PSA tests, the outputs are summed to the corresponding reference maps in which

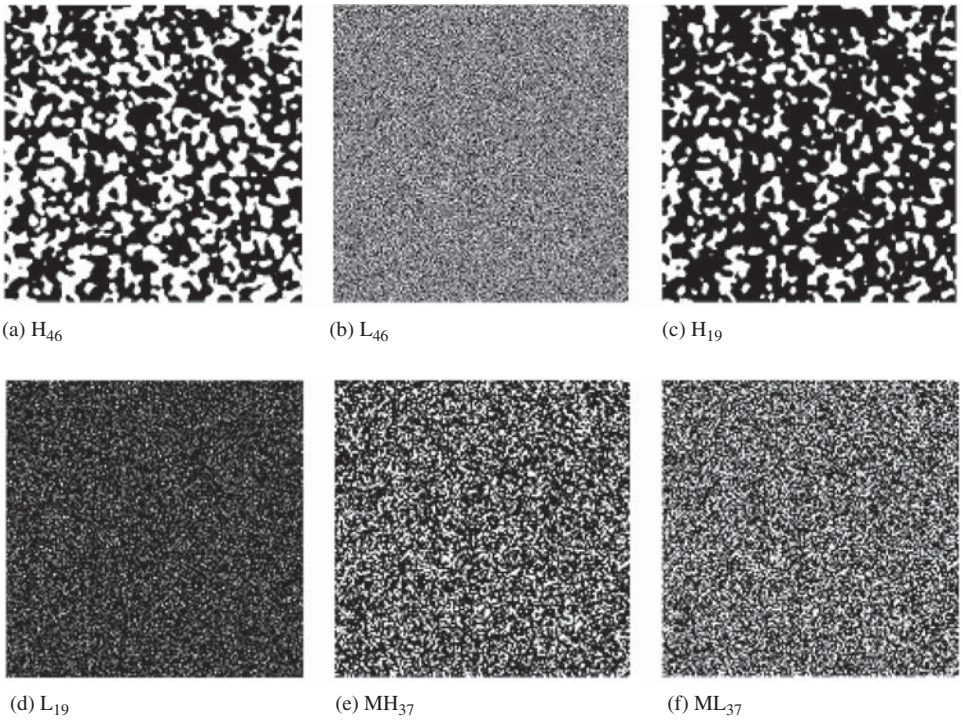


Figure 2. Simulated reference maps with different spatial autocorrelation and class proportions. (a) High spatial autocorrelation and low class proportion difference ($H_{46}$). (b) Low spatial autocorrelation and low class proportion difference ($L_{46}$). (c) High spatial autocorrelation and high class proportion difference ($H_{19}$). (d) Low spatial autocorrelation and high class proportion difference ($L_{19}$). (e) Medium high spatial autocorrelation and medium class proportion difference ($MH_{37}$). (f) Medium low spatial autocorrelation and medium class proportion difference ($ML_{37}$). Class '1' is black and '0' is white.

Table 1. Detailed configuration of reference maps.

| Reference map | Description | Spatial auto correlation (*Moran's I*) | Class proportion(%) '0' | '1' |
|---|---|---|---|---|
| $H_{46}$ | High spatial autocorrelation<br>Low class proportion difference | 0.895 | 40 | 60 |
| $L_{46}$ | Low spatial autocorrelation<br>Low class proportion difference | 0.056 | 40 | 60 |
| $H_{19}$ | High spatial autocorrelation<br>High class proportion difference | 0.877 | 10 | 90 |
| $L_{19}$ | Low spatial autocorrelation<br>High class proportion difference | 0.176 | 10 | 90 |
| $MH_{37}$ | Medium high spatial autocorrelation<br>Medium class proportion difference | 0.634 | 28 | 72 |
| $ML_{37}$ | Medium low spatial autocorrelation<br>Medium class proportion difference | 0.509 | 33 | 67 |

class labels '1' and '0' have been reclassified. The resulting raster accuracy maps provide four new class labels that are summarized into conventional error/confusion matrices that summarize the number of correct class matches and errors of commission and omission for the two classes. Overall (OA), producer (PA) and user (UA) accuracy percentages are also provided for each class.

Block majority filtering (BMF) is the benchmark or accuracy control to assess the relative efficiency and accuracy of the PSA at each zoom factor being tested. Block majority is a simple aggregation approach that partitions the input raster (in this case reference maps) into blocks and finds the majority value (value appearing most often) for the cells (defined by the neighbourhood parameters) within those blocks. The resultant majority value is assigned to every cell, at the original input cell size, in the corresponding output raster block. Square blocks correspond in size to the zoom factors being tested. With the

PSA being employed to sub-pixel map class proportions based on aggregations of the same reference maps using the same set of zoom factors we develop an intuitive accuracy comparison and control.

In past research, overall accuracies or PCC values of all pixels are used to assess the accuracy of the PSA outputs. This accuracy measure potentially overestimates the performance of PSA by including both pure and mixed pixels. If a pixel is pure, all sub-pixels are assigned to one class and sub-pixel mapping is purely geometric with no pixel-swapping taking place. Sub-pixel mapping is thus warranted only within mixed pixels and in this study pure and mixed pixels are consequently identified and accuracies of the PSA's ability to sub-pixel map within these pixels evaluated. To isolate mixed pixel accuracies, the aggregated reference maps are reclassified to produce pure and mixed pixel raster masks. These masks are then used to clip the accuracy maps produced from the earlier tests. This process isolates the accuracies distributed within mixed and pure pixels of the maps generated by the PSA.



## 4. Results and discussion

Study results are discussed for each of the four test groups: (1) PSA settings; (2) spatial autocorrelation; (3) class proportion; and (4) overall and mixed pixels within input maps.

In terms of setting optimums, Table 2 presents the optimum range (*a*) and neighbour depth settings and the overall accuracies achieved in the PSA runs upon the high and low spatial autocorrelation reference maps ($H_{46}$ and $L_{46}$) at zoom factors of 2, 4 and 10. Figures 3 and 4 display the OA trend relative to the range (*a*) and neighbour depth settings for maps $H_{46}$ and $L_{46}$ at a zoom factor of 10, respectively, and indicate the response of spatial autocorrelation levels to differing neighbour depth settings.

In Table 2, accuracies and setting optimums coincide with the results of Atkinson (2005), Makido and Qi (2005) and Makido and Shortridge (2005) whereby the optimal (*a*) and neighbour depth settings, at which the accuracy of PSA output is maximized, generally increase with increasing zoom factors in both low and high spatially autocorrelated maps.

It is clear from the OA of $H_{46}$ and $L_{46}$ maps in Table 2 that at generally the same neighbour depth, range (*a*) and zoom settings, the PSA performs, as expected, more accurately on the map with a high spatial autocorrelation than the map possessing a low spatial autocorrelation. The OA of PSA output is higher than 86% in $H_{46}$ at a zoom factor of 10 for all settings as depicted in Figure 3, whereas the OA in $L_{46}$ is lower than 53% and less than the accuracy of the BMF depicted in Figure 4. Of interest is how the larger neighbour depth settings of 4 and 6 improve PSA performance in map $H_{46}$ over a neighbour depth setting of 2, whereas a neighbour depth setting of 8 generally reduced accuracies at all range settings except a range setting of 2. This trend is not evident in $L_{46}$, yet, the optimal settings achieving the highest accuracy are the same as in map $H_{46}$. These trends are noteworthy to consider when selecting PSA optimums for future PSA applications.

From the next test group, Table 3 lists the overall (OA), producer (PA) and user (UA) accuracies from the most accurate PSA output maps for each of the respective reference and BMF maps at the zoom factors of 2, 4 and 10. The known trend that the PSA achieves higher accuracy upon high spatially autocorrelated maps compared with low autocorrelated maps is further validated in the other set of high and low spatially autocorrelated maps ($H_{19}$ and $L_{19}$). Figures 5 and 6 display the reference map (a), the PSA output map (b), the BMF map (c) and the accuracy map (d) for $H_{46}$ and $L_{46}$, respectively. These figures enable a visual comparison of reference and output map pattern and error distribution. In Figures 5 and 6 accuracy maps (d) are zoomed in six times (x's), within the quadrant location identified by a box on the reference map (a), to better view the spatial distribution of error.

In the figures it is not surprising that the majority of error is located amongst mixed pixels bordering pure pixels in all maps. The PSA achieves a higher OA than the BMF in high autocorrelated maps. At the zoom factor of 2 the PSA achieved the OA of 99.68% for $H_{46}$, 99.70% for $H_{19}$ and 95.16% for $MH_{37}$, whereas the corresponding BMF's accuracies are 98.45% for $H_{46}$, 98.67% for $H_{19}$ and 94.59%

Table 2. PSA setting optimums given overall accuracies for the H46 and L46 maps.

| Ref. map and spatial autocorrelation level | Zoom Factor | PSA optimums | | Overall accuracy (%) |
|---|---|---|---|---|
| | | Range (*a*) | Neighbour depth | |
| $H_{46}$–high | 2 | 2 | 2 | 99.68 |
| | 4 | 2 | 2 | 97.98 |
| | 10 | 7 | 4 | 89.40 |
| $L_{46}$–low | 2 | 2 | 2 | 66.97 |
| | 4 | 2 | 4 | 55.41 |
| | 10 | 7 | 4 | 52.33 |

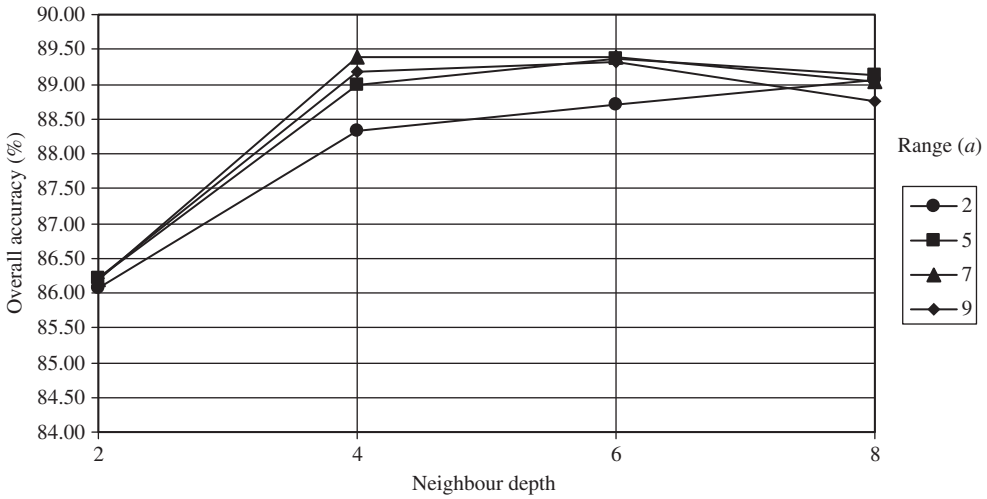


Figure 3. Overall accuracy of PSA output under varying neighbour depth and range settings using the $H_{46}$ reference map (high spatial autocorrelation and low class proportion difference) at a zoom factor of 10.



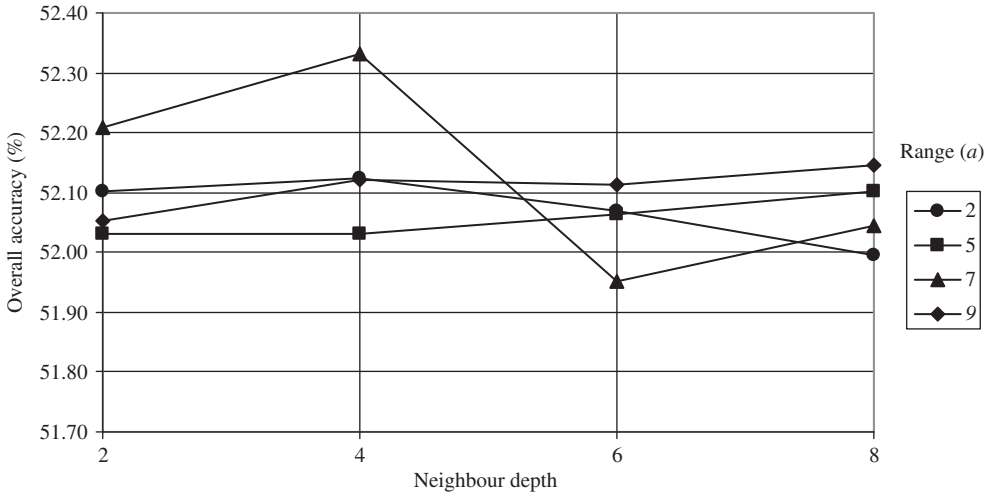


Figure 4. Overall accuracy of PSA output under varying neighbour depth and range settings using the $L_{46}$ reference map (low spatial autocorrelation and low class proportion difference) at a zoom factor of 10.

Table 3. Overall accuracy of outputs from optimum PSA settings and block majority filtering (BMF) for maps at zoom factors 2, 4 and 10.

| | Overall accuracy (%) | | | | | |
|---|---|---|---|---|---|---|
| | Zoom factor 2 | | Zoom factor 4 | | Zoom factor 10 | |
| Map | PSA | BMF | PSA | BMF | PSA | BMF |
| $H_{46}$ | 99.68 | 98.45 | 97.98 | 93.71 | 89.40 | 82.78 |
| $L_{46}$ | 66.97 | 82.25 | 56.17 | 65.50 | 52.24 | 59.00 |
| $H_{19}$ | 99.70 | 98.67 | 98.32 | 94.56 | 91.13 | 85.36 |
| $L_{19}$ | 90.02 | 94.19 | 84.89 | 89.93 | 81.99 | 89.68 |
| $MH_{37}$ | 95.16 | 94.59 | 83.70 | 82.99 | 64.79 | 73.09 |
| $ML_{37}$ | 89.36 | 91.98 | 73.63 | 77.51 | 59.11 | 68.34 |

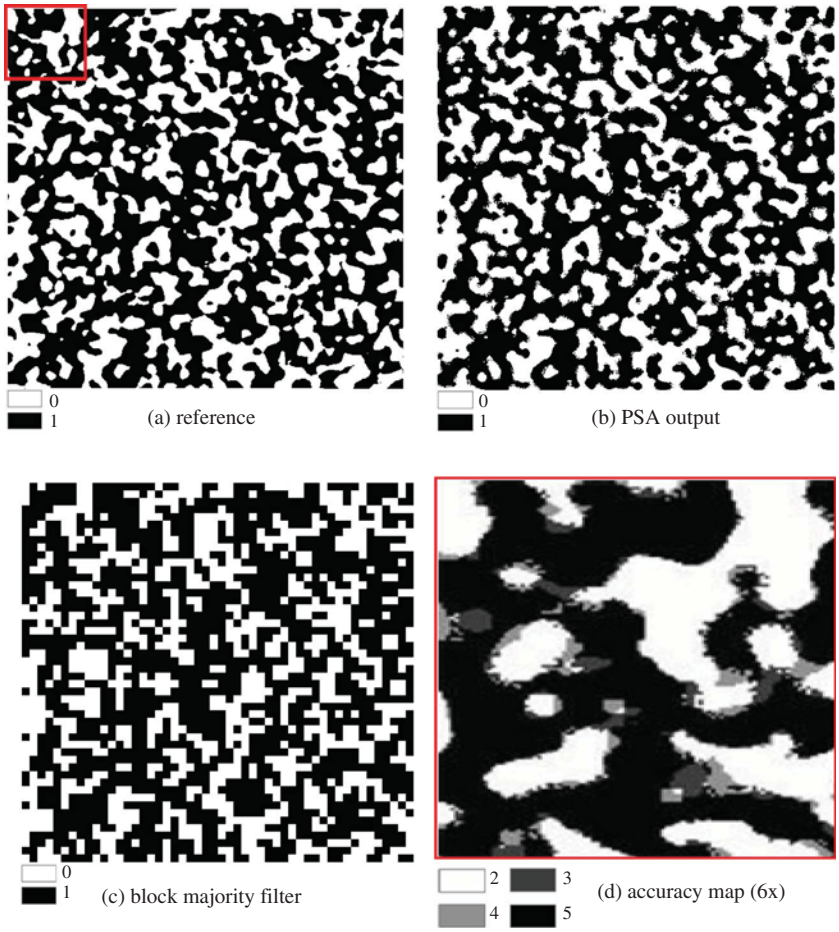


Figure 5. Comparison of the reference map to outputs from the PSA and BMF for high class spatial autocorrelation and low class proportion map $H_{46}$ at zoom factor of 10. In the accuracy map (d): white pixels ('2') are '0's which are correctly mapped by the PSA; black pixels ('5') are '1's' that are correctly mapped. Lighter grey pixels ('4') are '1's' mapped as '0's'; and darker grey pixels ('3') are '0's mapped as '1's).



for $MH_{37}$. The advantage of PSA becomes more evident as the zoom factor increases in high spatially autocorrelated maps. At the zoom factor of 10 the OA from PSA is 89.40% for $H_{46}$ and 91.13% for $H_{19}$ whereas the corresponding BMF accuracies are 82.78% and 69.91%, respectively. The map in Figure 5(b) looks more similar to the reference map in Figure 5(a) than the map in Figure 5(c) visibly demonstrating that the PSA outperforms the BMF as expected in a high autocorrelation map ($H_{46}$). However, again as expected, this is not true in low spatially autocorrelated maps. The OA of PSA at the zoom factor of 2 is 66.97% for $L_{46}$, 90.02% for $L_{19}$ and 89.36% for $ML_{37}$, whereas the corresponding accuracies of the BMF are 82.25%, 94.19% and 91.98%. From Figure 6, it can also be seen that the PSA has performed poorly on the low spatially autocorrelated map ($L_{46}$) with the resulting map (b) forming more pure and contiguous pixel zones compared with the reference map. The OA of PSA outputs at a zoom factor of 10 is less than the BMF for all low and medium level spatial autocorrelation reference maps.

The above results indicate that sub-pixel mapping employing the PSA is substantially less accurate on a low spatial autocorrelation map. For example, at a zoom factor of 4 under the same PSA settings and class proportions an OA difference of up to 42% can occur between the PSA outputs for maps $H_{46}$ and $L_{46}$. Maps with high spatial autocorrelation can be much more accurately mapped by the PSA, whereas the BMF can be used to achieve a similar or better OA performance to the PSA on maps with low spatial autocorrelation. These findings coincide with the manner in which the PSA functions by maximizing spatial autocorrelation in input images.

Referring back to Table 3, comparing the accuracy results from PSA outputs on maps with different class proportions, it is clear that on high spatial autocorrelation maps class proportion has less impact on PSA accuracy. The PSA achieves very similar high accuracies in maps $H_{46}$ (99.68%), $H_{19}$ (99.70%) and $MH_{37}$ (95.16%) despite the difference in their class proportions. However, the PSA accuracy shows a great variation on low spatially

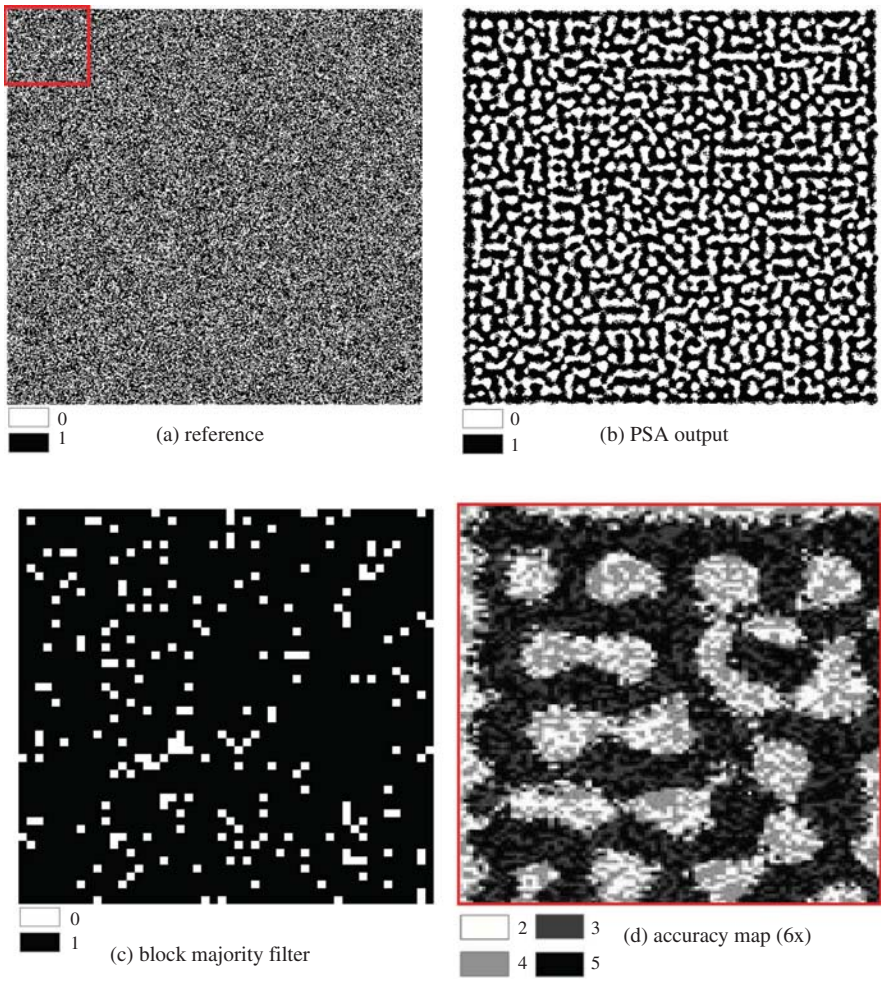


Figure 6. Comparison of the reference map to outputs from the PSA and BMF for low class spatial autocorrelation and low proportion difference map $L_{46}$ at zoom factor of 10. In the accuracy map (d): white pixels ('2') are '0's which are correctly mapped by the PSA; black pixels ('5') are '1's' that are correctly mapped. Lighter grey pixels ('4') are '1's' mapped as '0's'; and darker grey pixels ('3') are '0's mapped as '1's.



autocorrelated maps with different class proportions. The OA of PSA output for reference maps $L_{19}$, $ML_{37}$ and $L_{46}$ at zoom factor 2 are 90.02%, 89.36% and 66.97%, respectively. This trend remains consistent across zoom factors 4 and 10 and indicates that in low spatial autocorrelation maps the PSA performs better as class proportion difference increases.

Table 4, at a zoom factor of 2, provides further test outcomes regarding the influence of class proportion, while also providing overall, producer and user accuracies of the individual classes. The frequency dominant class (i.e. the higher proportion of image pixels of a particular class) always scores higher producer and user accuracies. With the PSA swapping classes between sub-pixels to maximize spatial autocorrelation, the results of this test provide evidence that frequency dominant classes are targeted and achieve higher accuracies at the expense of accuracy within the less dominant class. Holding all other factors constant, this accuracy margin increases between the majority and minority class moving from the high to low spatial autocorrelation maps. Similar to the OA, the PA and UA of individual classes '0' and '1' are very similar on high spatially autocorrelated maps $H_{46}$, $H_{19}$ and $MH_{37}$ at a zoom factor of 2. However, the difference between PAs and UAs of class '0' and class '1' increases dramatically in low spatially autocorrelated maps when moving from $L_{19}$ (*Moran's* $I = 0.176$) $ML_{37}$ (*Moran's* $I = 0.509$) to $L_{46}$ (*Moran's* $I = 0.056$).

To examine the PSA's performance within mixed pixels, these pixels are isolated from pure pixels in all the accuracy maps. In Table 4 the overall and individual class's accuracy of all pixels (which include both pure and mixed pixels) and mixed pixels alone at the zoom factor of 2 are listed. As expected, the OA within

Table 4. Accuracy comparison for overall and mixed pixel outputs from the PSA and the block majority filtering (BMF) at zoom factor of 2.

| Mixed pixels[1](%) | | All pixels | | | | | Mixed pixels | | | | |
|---|---|---|---|---|---|---|---|---|---|---|---|
| | | | Class '1' | | Class '0' | | | Class '1' | | Class '0' | |
| Map | Method | OA | PA | UA | PA | UA | OA | PA | UA | PA | UA |
| 10.00 | PSA | 99.68 | 99.73 | 99.73 | 99.61 | 99.61 | 96.79 | 96.83 | 96.83 | 96.76 | 96.76 |
| | BMF | 98.45 | 98.76 | 98.66 | 98.00 | 98.15 | 75.65 | 77.69 | 75.31 | 73.54 | 76.03 |
| 80.52 | PSA | 66.97 | 71.74 | 71.74 | 60.25 | 60.25 | 58.98 | 61.62 | 61.62 | 55.94 | 55.94 |
| | BMF | 82.25 | 89.12 | 83.6 | 70.76 | 79.55 | 74.93 | 82.76 | 74.95 | 65.05 | 74.91 |
| 8.59 | PSA | 99.70 | 99.79 | 99.79 | 99.47 | 99.47 | 96.50 | 96.56 | 96.56 | 96.43 | 96.43 |
| | BMF | 98.67 | 99.14 | 99.03 | 97.44 | 97.72 | 75.08 | 77.46 | 74.71 | 72.59 | 75.50 |
| 28.27 | PSA | 90.02 | 94.44 | 94.44 | 51.63 | 51.63 | 64.70 | 94.44 | 94.44 | 51.63 | 51.63 |
| | BMF | 94.19 | 99.39 | 94.44 | 51.63 | 80.26 | 74.63 | 96.29 | 74.80 | 23.69 | 73.10 |
| 29.56 | PSA | 95.16 | 96.63 | 96.63 | 91.39 | 91.39 | 83.62 | 84.65 | 84.65 | 82.45 | 82.45 |
| | BMF | 94.59 | 97.10 | 95.69 | 87.31 | 91.22 | 74.38 | 81.41 | 74.40 | 65.81 | 74.36 |
| 42.88 | PSA | 89.36 | 92.10 | 92.1 | 83.73 | 83.73 | 75.20 | 76.87 | 76.87 | 73.26 | 73.26 |
| | BMF | 91.98 | 95.62 | 93.19 | 83.23 | 88.80 | 78.80 | 86.16 | 78.07 | 69.54 | 79.97 |

[1]Percentage of sub-pixels in reference maps falling within mixed pixels of spatially aggregated reference maps as input to the PSA.



mixed pixels consistently scores much less than the overall accuracies across all pixels. This difference ranges from 2.89% ($H_{46}$) to 25.32% ($L_{19}$) at the zoom factor of 2. Furthermore, the difference between the OA within mixed pixels relative to the overall accuracies across all pixels increases as spatial autocorrelation levels decrease and the class proportion difference increase. This indicates that for maps with high spatial autocorrelation, the accuracy of all pixels is fairly representative of the performance of the PSA even within mixed pixels. On the contrary, for maps with a low spatial autocorrelation, the accuracy across all pixels greatly overestimates the performance of PSA and notably within mixed pixels. This trend is strengthened with large class proportion differences.

Although the outputs from the BMF on the high spatial autocorrelated maps show similar overall and individual accuracies for all pixels to those of the PSA, this similarity does not hold within mixed pixels. For example, at the zoom factor of 2, the outputs from PSA and BMF for map $H_{46}$ exhibit overall accuracies of 99.68% and 98.45% across all pixels, respectively. However, after excluding pure pixels, the OA of mixed pixels is 96.79% for the PSA and 75.65% for the BMF. With a difference between the mixed and overall pixel accuracies of 22.14% for the PSA and 1.23% for the BMF, respectively, the PSA is shown to perform significantly better than the BMF within mixed pixels.

The overriding performance of the PSA on maps with high spatial autocorrelation is even more evident based on the individual accuracies of classes within mixed pixels. For maps $H_{46}$, $H_{19}$ and $MH_{37}$, the individual accuracy of the PSA within both classes for mixed pixels is over 82%, irregardless of class proportion. The BMF scores below 82%, with most accuracies ranging from 65% to 78%, for the corresponding classes within mixed pixels. Upon low spatial autocorrelated maps, the PSA consistently scores lower individual accuracies compared with the BMF within mixed pixels.

These findings further demonstrate and validate the significance of spatial autocorrelation to the PSA's performance in accordance to the algorithm being premised upon maximizing spatial autocorrelation at the target resolution. True to prior research (Makido and Qi 2005, Makido and Shortridge 2005), on maps with low spatial autocorrelation levels the PSA performs poorly, and in this case, relative to the BMF. With spatial autocorrelation on maps increasing to the middle level, the BMF and PSA start to achieve similar overall and individual class accuracies and when spatial autocorrelation levels are high the PSA outperforms the BMF. Based on test results, the point at which the BMF begins to score better than the PSA, based on spatial autocorrelation, lies upon maps with a *Moran's I* value below 0.63 (map $MH_{37}$). The corollary being that a general minimum level of spatial autocorrelation required for accurate sub-pixel mapping in this study using the PSA lies at and above the same *Moran's I* value. Further testing on maps possessing a finer resolution of *Moran's I* values between 0.634 and 0.509 can confirm a more precise spatial autocorrelation cut-off value.

## 5. Conclusion

This study isolates and further reveals the performance and accuracy of a popular sub-pixel mapping algorithm – the pixel-swapping algorithm (PSA) – to sub-pixel map class proportion images. A series of tests are conducted at differing zoom factors and algorithm settings upon a group of input images simulating differing spatial autocorrelation, class proportion and mixed pixel compositions.

Findings demonstrate the correlation between and quantify the importance of spatial autocorrelation (*Moran's I*), percentage of mixed pixels, class proportion difference and zoom factor upon the accuracy of outputs from the PSA.

Specifically, the primary input image factors positively impacting the PSA's accuracy are initial spatial autocorrelation and class proportion levels. This finding is intuitive with the working of the PSA that swaps class positions in mixed pixels to maximize spatial autocorrelation usually comprised amongst the dominant or more frequent class. As such, if an input image structure is too random and the classes are close in proportion the PSA can be ineffective. Remaining factors having a negative impact on the PSA's accuracy are increasing zoom factors and greater numbers of mixed pixels in input images. These relationships are also logical to the workings of the PSA where larger zoom factors result in greater divergence and a commensurate loss of spatial autocorrelation over distance from the original input image/map resolutions exacerbated when the PSA is truly performing within a greater number of mixed pixels.

The majority of error when employing the PSA is situated within mixed pixels, which consistently exhibit overall accuracies lower than the overall accuracies amongst all image pixels comprising a given map. The difference in OA of the PSA between all map pixels and within mixed map pixels alone can be over 20%. Based on this finding, the OA or PCC measure, which has been conventionally applied in past research, has potentially overestimated the accuracy and performance of the PSA by including accuracies of 100% within pure pixels that forgo sub-pixel swapping. The PSA, in general, accurately sub-pixel mapped, relative to block majority filtering, input images with an approximate minimum spatial autocorrelation at a *Moran's I* of 0.63, a maximum of 30% mixed pixels relative to entire image pixels, a difference in class proportions greater than 40% and at zoom factors below 10.

In terms of future research, it is acknowledged that within real images subject to natural processes, spatial autocorrelation is variable across zones, regions or spatial extents with structure sizes related to spatial resolution. In these cases, such 'regional spatial autocorrelation variation' would be best measured locally to determine areas of spatial autocorrelation homogeneity to guide PSA application, notably, when extracting or sub-pixel mapping *a priori* defined objects or structures. With this in mind, structure size-to-cell size ratio and PSA accuracy can be isolated as future work. Nonetheless, the viability and degree to which the PSA is expected to improve accuracy within these regions is still contingent upon minimum spatial autocorrelation and appropriate image structure levels as identified from the globally derived measures within this study.

Additionally, future amendments to the PSA and other sub-pixel mapping algorithms to accommodate multiple classes in classified imagery can better target eligible imagery cognizant of approximate minimum spatial autocorrelation and class proportion levels, a maximum percentage of mixed pixels and appropriate zoom factors. Sub-pixel mapping efforts can also be focused solely on mixed pixels by using processing masks. Pure pixels can simply be geometrically mapped. Also a convergence criterion measuring the accuracy of targeted shapes and/or objects in the PSA output map may be investigated as a processing stopping rule as opposed to a simple number of iterations setting. The accuracy of and processing efficiency to produce the resulting sub-pixel mapped imagery will likely be increased.

**Acknowledgements**

The authors recognize and thank the Department of Geography and the R. Samvel McLaughlin fellowship at Queen's University, the Ontario Graduate Scholarship Program, and the National Science and Engineering Research Council (NSERC) of Canada for the collective academic funding to enable this research. The authors also thank anonymous reviewers for their insights, constructive comments and shared research wisdom.

**References**

Atkinson, P.M., 2005. Sub-pixel target mapping from soft-classified, remotely sensed imagery. *Photogrammetric Engineering and Remote Sensing*, 71 (7), 839–846.

Atkinson, P.M., Cutler, M.E.J., and Lewis, H., 1997. Mapping sub-pixel proportional land cover with AVHRR images. *International Journal of Remote Sensing*, 18, 917–935.

Blöshchl, G. and Sivapalan, M., 1995. Scale issues in hydrological modeling: a review. Hydrological Processes, 9, 251–290.

Boucher, A. and Kyriakidis, P.C., 2006. Super-resolution land cover mapping with indicator geostatistics. *Remote Sensing of Environment*, 104, 264–282.

Chen, D. and H. Wei, 2009. The effect of spatial autocorrelation and class proportion on the accuracy measures from different sampling designs. *ISPRS Journal of Photogrammetry and Remote Sensing*, 64 (2), 140–150.

Chiles, J.P. and Delfiner, P., 1999. *Geostatistics: modeling spatial uncertainty*. New York: Wiley and Sons.

Curran, P.J. and Atkinson, P.M., 1998. Geostatistics and remote sensing. *Progress in Physical Geography*, 22, 61–78.

Foody, G.M., 1998. Sharpening fuzzy classification output to refine the representation of sub-pixel land cover distribution. *International Journal of Remote Sensing*, 19, 2593–2599.

Gavin, J. and Jennison, C., 1997. A sub-pixel image restoration algorithm. *Journal of Computational and Graphical Statistics*, 6, 182–201.

Goovaerts, P. 1997. *Geostatistics for natural resources evaluation*. New York: Oxford University Press.

Kasetkasem, T., Arora, M.K., and Varshney, P.K., 2005. Super-resolution land cover mapping using a Markov random field based approach. *Remote Sensing of Environment (RSE)*, 96, 302–314.

Lu, D. and Weng, Q., 2007. A survey of image classification methods and techniques for improving classification performance. *International Journal of Remote Sensing*, 28, 823–870.

Makido, Y. and Shortridge, A., 2005. Land cover mapping at sub-pixel scales: unravelling the mixed pixel. *In: 8th international geocomputation conference. Proceedings*, 2005, 1, 1–12.

Makido, Y. and Qi, J., 2005. Land cover mapping at sub-pixel scales using remote sensing imagery. *In: Geoscience and*

*remote sensing symposium,* 2005. *IGARSS '05. Proceedings. IEEE International*, 2005, 1, 514–516.

Matheron, G., 1965. *Les variables réionalisées et leur estimation*. Paris: Masson.

Mertens, K.C., *et al*., 2004. Direct Sub-pixel mapping exploiting spatial dependence. *In: Geoscience and remote sensing symposium. Proceedings of IGARSS '04. IEEE International*, 2004, 3046–3049.

Mertens, K.C., *et al*., 2006. A sub-pixel mapping algorithm based on sub-pixel/pixel spatial attraction models. *International Journal of Remote Sensing*, 27, 3293–3310.

Moran, P.A.P., 1948. The interpretation of statistical maps. *Journal of the Royal Statistical Society Series B*, 10, 243–251.

Muslim, A.M., Foody, G.M., and Atkinson, P.M., 2006. Localized soft classification for super-resolution mapping of the shoreline. *International Journal of Remote Sensing*, 27, 2271–2285.

Tatem, A.J., *et al*., 2001. Super-resolution target identification from remotely sensed images using a Hopfield neural network. *IEEE Transactions on Geoscience and Remote Sensing*, 39, 781–796.

Thornton, M.W., Atkinson, P.M., and Holland, D.A., 2006. Sub-pixel mapping of rural land cover objects from fine spatial resolution satellite sensor imagery using super-resolution pixel-swapping. *International Journal of Remote Sensing*, 27, 473–491.

Thornton, M.W., Atkinson, P.M., and Holland, D.A., 2007. A linearised pixel-swapping method for mapping rural linear land cover features from fine spatial resolution remotely sensed imagery. *Computers and Geosicences*, 33, 1261–1272.

Verhoeye, J. and De Wulf, R.R., 2002. Land cover mapping at the sub-pixel scale using linear optimization techniques. *Remote Sensing of Environment*, 79, 96–104.